Dynamic Analysis of 4-Node Degenerated Shell Element with Updated Thickness

Dalia Calneryte(✉) and Rimantas Barauskas

Faculty of Informatics, Department of Applied Informatics, Kaunas University of Technology, Studentu, 50-407 Kaunas, Lithuania
{dalia.calneryte, rimantas.barauskas}@ktu.lt

Abstract. There is a variety of approaches available to model the large strain behavior of shells in dynamic analysis. This article examines the significance of the iterative shell thickness update for the 4-node degenerated shell element with Reissner-Mindlin assumptions. The updated Lagrangian formulation in explicit and implicit dynamic integration schemes is described. The rigid link correction is employed to reduce the warp of the element. Numerical examples including dynamic analysis of fixed beam and pinched cylinder are presented. The results show that significance of the thickness update occur for the large strains.

Keywords: Updated Lagrangian formulation · 4-node degenerated shell element · Bathe integration scheme · Nonlinear dynamic analysis

1 Introduction

Dynamic finite element analysis is widely used to investigate the response of the structure under the desirable load and boundary conditions. If the dimensions of the structure are significantly small in one direction compared with others, the shell elements are convenient in finite element model simulation. Shell elements are classified into three main groups: the curved shell elements based on classical shell theories, degenerated shell elements and flat shell elements combining properties of membrane and bending plate [6]. The 4-node degenerated shell element is considered in this paper.

If large strain behavior is simulated, the change in shell thickness should be considered. Three different approaches applied to model the large strain behavior of shells are discussed in [9]. The simplest and the most cost-efficient approach is to update the thickness iteratively. The element thickness is updated to ensure the incompressible behavior for the thin basic shell triangles in [7] using this approach. The same update scheme is applied for the thick 4-node shell element in this paper. Other approaches presented in [4] consist of using solid elements or three dimensional higher order shell elements with at least 7 parameters. However, evaluation of additional parameters increase computational cost of the model.

The aim of this paper is to examine the significance of the iterative shell thickness update in dynamic behavior. Damping effects are not considered in the research. Firstly, the 4-node degenerated shell element with the rigid link correction and transformation from global to local system in case of the warped element is described. Secondly, the updated Lagrangian formulation with explicit and implicit integration

G. Dregvaite and R. Damasevicius (Eds.): ICIST 2015, CCIS 538, pp. 592–603, 2015.
DOI: 10.1007/978-3-319-24770-0_50

schemes is presented. Finally, the numerical examples including beam with fixed ends and pinched cylinder with rigid diaphragms at the ends are proposed to illustrate the effects of thickness update.

2 4-Node Degenerated Shell Element

Degenerated shell element was derived from the solid element by defining all displacements (translational and rotational) with respect to the mid-surface [8]. Any shell element is defined by material properties, mid-surface normals at each node, geometry and thickness of the element [12]. Shear strains γ_{yz}, γ_{zx} are considered to be not equal to zero for the thick shell with Reissner-Mindlin assumptions. Reissner-Mindlin theory states that a straight line normal to the undeformed middle surface remains straight but not necessarily orthogonal to the middle plane after deformation [8]. Shear correction factor $\kappa = 5/6$ is employed to compensate the error due to the assumption of constant shear strains within plate thickness although the shear stresses σ_{yz}, σ_{zx} are quadratic functions of thickness coordinate [11].

A 2 × 2 Gauss integration rule is employed to obtain stiffness matrix and internal force vector for the 4 node element in plane. Reduced through-thickness integration is used to avoid shear locking.

2.1 Transformation to Local Coordinates

Local coordinate system is calculated with respect to the mean plane of the element. Means plane passes through all mid-side points of the element (12, 23, 34, 41 in Fig. 1) [6] and is defined by a normal vector and a point through which it passes [13]. If all nodes of the elements are located in one plane, the mean plane coincides with the element. Vectors $\mathbf{V}_{12,34}$ connecting mid-side points 12 and 34 and $\mathbf{V}_{41,23}$ connecting mid-side points 41 and 23 are defined to calculate vector $\mathbf{V_3}$ normal to the mean plane:

$$\mathbf{V_3} = \mathbf{V}_{41,23} \times \mathbf{V}_{12,34}. \tag{1}$$

$\mathbf{V_1}$ is perpendicular to $\mathbf{V_3}$ and parallel to $\mathbf{V}_{41,23}$. The third vector $\mathbf{V_2}$ employed to define local coordinate system is calculated as follows:

$$\mathbf{V_2} = \mathbf{V_3} \times \mathbf{V_1}. \tag{2}$$

Local axes $\mathbf{x}$, $\mathbf{y}$, $\mathbf{z}$ in the global system correspond to normalized orthogonal vectors $\mathbf{V_1}$, $\mathbf{V_2}$, $\mathbf{V_3}$ at the center of the mean plane of element [13] and are used to transform variables between local and global axes [12].

2.2 Shell Formulation

Any point of shell element can be defined by nodal coordinates, shell thickness h and a normalized vector $\mathbf{v}_{3k}$ connecting upper and lower surfaces at the kth node:

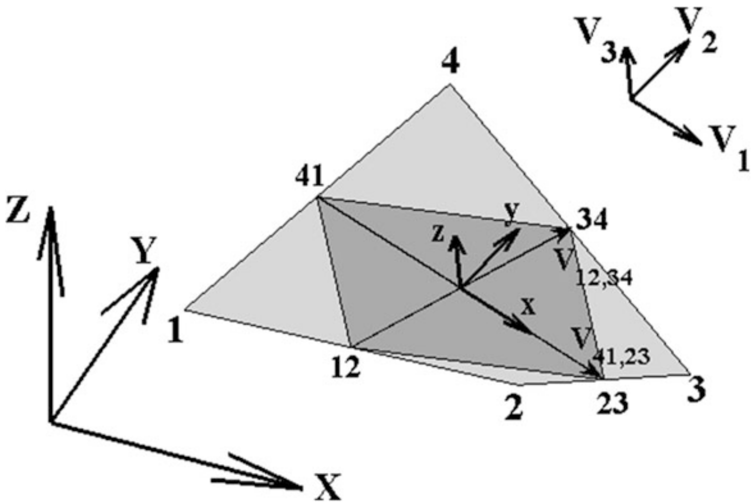

Fig. 1. Global and local coordinates of the warped shell element.

$$\begin{Bmatrix} x \\ y \\ z \end{Bmatrix} = \sum N_k(\xi,\eta) \cdot \left(\begin{Bmatrix} x_k \\ y_k \\ z_k \end{Bmatrix} + \frac{1}{2}\zeta\, h\, \mathbf{v}_{3k} \right), \tag{3}$$

where the shape function $N_k(\xi,\eta)$ is a bi-linear Lagrangian polynomial of the kth node and ζ is a linear coordinate in the thickness direction.

The displacements at each node of shell are uniquely defined by three translational displacements u, v, w and two rotations θ_x, θ_y about the vectors $\mathbf{v}_{1k}$ and $\mathbf{v}_{2k}$ orthogonal to vector $\mathbf{v}_{3k}$. The drilling degree of freedom θ_z (rotation about the $\mathbf{z}$ axis) is added to apply a unified procedure for the transformation of translational and rotational displacements from local to global coordinate system [12]. This degree of freedom constrained in the global system. Displacements at any point of the element are calculated according the formula:

$$\begin{Bmatrix} u \\ v \\ w \end{Bmatrix} = \sum N_k(\xi,\eta) \cdot \begin{Bmatrix} u_k \\ v_k \\ w_k \end{Bmatrix} + \zeta \sum N_k(\xi,\eta) \cdot [\mathbf{g}_{1k} \quad \mathbf{g}_{2k}] \begin{Bmatrix} \theta_{xk} \\ \theta_{yk} \end{Bmatrix}, \tag{4}$$

where $\mathbf{g}_{1k} = -\frac{h}{2}\mathbf{v}_{2k}$, $\mathbf{g}_{2k} = \frac{h}{2}\mathbf{v}_{1k}$ [1].

2.3 Rigid Link Correction for the Warped Shell Element

The initial mesh of the analyzed structure consists of flat 4-node shell elements. The stiffness matrix $\mathbf{K}$ is calculated with the assumption that all four nodes of the element are in the same plane. However, if the initial structure assembled of elements is curved, the initial geometry of element is often warped. Moreover, if out-of-plane loads of the different magnitude are applied on the nodes of the element during the simulation, the element warps and the flat element assumption is not satisfied in later calculations. The rigid link correction is applied to the stiffness matrix of the warped element before the transformation to the global coordinate system [6]:

$$\mathbf{K}_{local} = \mathbf{W}\mathbf{K}_{flat}\mathbf{W}^T, \tag{5}$$

where $\mathbf{W}$ is a projection matrix to the mid-plane of the element consisting four diagonally located blocks $\mathbf{W}_k$, $k = \overline{1,4}$:

$$\mathbf{W}_k = \begin{bmatrix} 1 & 0 & 0 & 0 & 0 & 0 \\ 0 & 1 & 0 & 0 & 0 & 0 \\ 0 & 0 & 1 & 0 & 0 & 0 \\ d_k & 0 & 0 & 1 & 0 & 0 \\ 0 & d_k & 0 & 0 & 1 & 0 \\ 0 & 0 & 0 & 0 & 0 & 1 \end{bmatrix} \tag{6}$$

and d_k is the offset of the kth node with respect to the mid-plane.

3 Updated Lagrangian Formulation in FEM Dynamic Analysis

Updated Lagrangian formulation relates 2nd Piola-Kirchhoff stress to Green-Lagrange strain referred to the configuration at time t [1]. Explicit and implicit integration techniques can be employed to get the response of structure at time t. The central difference scheme employed in explicit analysis has a low computational cost but is only conditionally stable and requires a small time step in nonlinear analysis when large deformations are considered. On the contrary, a composite implicit two-substep time integration scheme proposed in [2, 3] is stable in both linear and nonlinear analysis.

A superscript on the left of the variable indicates the configuration the quantity occurs and the subscript on the left indicates the reference configuration [1]. It is assumed that all variables are known at time t and the variables at time $t + \Delta t$ are computed. All variables but mass matrix are evaluated at the last known configuration at time t [2, 3]. The diagonal mass matrix $\mathbf{M}$ is calculated once with respect to the initial configuration. Mass matrix for the 4-node shell element consists of 4 diagonally located blocks $\mathbf{M}_k$, $k = \overline{1,4}$ [10]:

$$\mathbf{M}_k = \begin{bmatrix} m_u\mathbf{I}_{3\times3} & 0 \\ 0 & m_\theta\mathbf{I}_{3\times3} \end{bmatrix}, \; m_u = \frac{\rho A h}{4}, \; m_\theta = \frac{h^2}{12} m_u, \tag{7}$$

where $\mathbf{I}_{3\times3}$ is a 3×3 identity matrix, ρ is the density of the material, A is the area of the element, h is the thickness of the element.

The shell thickness ${}^{t+\Delta t}h$ is updated at each iteration for the implicit dynamic analysis and each time step for the explicit analysis [7]:

$$ {}^{t+\Delta t}h = \frac{{}^{t}A\,{}^{t}h}{{}^{t+\Delta t}A}, \tag{8} $$

where A is the area of the element.

3.1 Explicit Analysis

The equations of the motion solved in explicit analysis at time $t + \Delta t$ in the matrix form are:

$$ \mathbf{M} \cdot {}^{t+\Delta t}\ddot{\mathbf{U}} = {}^{t+\Delta t}\mathbf{R} - {}^{t+\Delta t}\mathbf{F}, \tag{9} $$

where $\mathbf{M}$ - mass matrix at the initial configuration, ${}^{t+\Delta t}\ddot{\mathbf{U}}$ - vector of accelerations, ${}^{t+\Delta t}\mathbf{R}$ - vector of external forces, ${}^{t+\Delta t}\mathbf{F}$ - vector of internal forces.The vector of internal forces ${}^{t+\Delta t}_{t+\Delta t}\mathbf{F}$ is evaluated using the formula:

$$ {}^{t+\Delta t}_{t+\Delta t}\mathbf{F} = \int\limits_{{}^{t+\Delta t}V} {}^{t+\Delta t}_{t+\Delta t}\mathbf{B}_L^T \cdot {}^{t+\Delta t}\mathbf{S}^{t+\Delta t} dV, \tag{10} $$

where $\mathbf{B}_L$ is strain – displacement matrix, such that $\boldsymbol{\varepsilon} = \mathbf{B}_L\mathbf{U}$ where $\boldsymbol{\varepsilon}$ is Green-Lagrange strain vector, $\mathbf{S}^T = \begin{bmatrix} \tau_{xx} & \tau_{yy} & \tau_{zz} & \tau_{xy} & \tau_{yz} & \tau_{zx} \end{bmatrix}$ is a 2nd Piola-Kirchhoff stress vector at time $t + \Delta t$ [1]. Displacements at the time $t + \Delta t$ are explicitly computed using central difference formula with constant time step Δt [5]:

$$ {}^{t+\Delta t}\mathbf{U} = \Delta t^2 \cdot \mathbf{M}^{-1} \cdot \left({}^{t+\Delta t}\mathbf{R} - {}^{t+\Delta t}\mathbf{F}\right) + 2 \cdot {}^{t}\mathbf{U} - {}^{t-\Delta t}\mathbf{U}. \tag{11} $$

3.2 Implicit Integration Scheme

The equation of the motion solved in implicit integration scheme for the Updated Lagrangian formulation is:

$$ {}^{t}_{t}\mathbf{K}^{(i-1)} \cdot \Delta\mathbf{U}^{(i)} = {}^{t+\Delta t}\mathbf{R} - {}^{t+\Delta t}_{t+\Delta t}\mathbf{F}^{(i-1)} - \mathbf{M} \cdot {}^{t+\Delta t}\ddot{\mathbf{U}}^{(i)}, \tag{12} $$

where $\mathbf{M}$ - mass matrix at the initial configuration, ${}^{t+\Delta t}\ddot{\mathbf{U}}$ - vector of acceleration, ${}^{t+\Delta t}\mathbf{R}$ - vector of external forces, ${}^{t+\Delta t}\mathbf{F}$ - vector of internal forces. Superscript on the right indicates the iteration the variable was obtained.

Stiffness matrix $\mathbf{K}$ is a sum of linear and nonlinear matrices [1]:

$$ {}_t^t\mathbf{K}_L = \int_{{}^tV} {}_t^t\mathbf{B}_L^T \mathbf{D} {}_t^t\mathbf{B}_L {}^t dV,\ {}_t^t\mathbf{K}_{NL} = \int_{{}^tV} {}_t^t\mathbf{B}_{NL}^T {}^t\mathbf{S} {}_t^t\mathbf{B}_{NL} {}^t dV, \tag{13} $$

where $\mathbf{D}$ is elasticity tensor for isotropic material, $\mathbf{S} = \begin{bmatrix} \tau_{xx}\mathrm{I}_3 & \tau_{xy}\mathrm{I}_3 & \tau_{xz}\mathrm{I}_3 \\ \tau_{xy}\mathrm{I}_3 & \tau_{yy}\mathrm{I}_3 & \tau_{yz}\mathrm{I}_3 \\ \tau_{xz}\mathrm{I}_3 & \tau_{yz}\mathrm{I}_3 & \tau_{zz}\mathrm{I}_3 \end{bmatrix}$, τ_{rs} are the components of a 2nd Piola-Kirchhoff stress, I_3 is 3×3 identity matrix, $\mathbf{B}_{NL}$ part for the kth node has the form:

$$ \mathbf{B}_{NLk} = \begin{bmatrix} N_{kx}^{'}\mathbf{I}_3 & \mathbf{g}_{1k}(\varsigma \cdot N_{kx}^{'} + \varsigma_x^{'} \cdot N_k) & \mathbf{g}_{2k}(\varsigma \cdot N_{kx}^{'} + \varsigma_x^{'} \cdot N_k) \\ N_{ky}^{'}\mathbf{I}_3 & \mathbf{g}_{1k}(\varsigma \cdot N_{ky}^{'} + \varsigma_y^{'} \cdot N_k) & \mathbf{g}_{2k}(\varsigma \cdot N_{ky}^{'} + \varsigma_y^{'} \cdot N_k) \\ N_{kz}^{'}\mathbf{I}_3 & \mathbf{g}_{1k}(\varsigma \cdot N_{kz}^{'} + \varsigma_z^{'} \cdot N_k) & \mathbf{g}_{2k}(\varsigma \cdot N_{kz}^{'} + \varsigma_z^{'} \cdot N_k) \end{bmatrix}. \tag{14} $$

The time step is divided to two equal substeps and the Newton-Raphson iterative scheme is employed to correct the solutions at each substep until the convergence is reached. Stiffness matrix $\mathbf{K}$ and internal force vector $\mathbf{F}$ are calculated at each iteration with respect to the corrected displacements. The trapezoidal rule is used to compute the solution in the 1st substep [3]:

$$ \begin{gathered} \left(\frac{16}{\Delta t^2}\mathbf{M} + {}^{t+\Delta t/2}\mathbf{K}^{(i-1)}\right)\Delta\mathbf{U}^{(i)} = \\ {}^{t+\Delta t/2}\mathbf{R} - {}^{t+\Delta t/2}\mathbf{F}^{(i-1)} - \mathbf{M}\left(\frac{16}{\Delta t^2}\left({}^{t+\Delta t/2}\mathbf{U}^{(i-1)} - {}^t\mathbf{U}\right) - \frac{8}{\Delta t}{}^t\dot{\mathbf{U}} - {}^t\ddot{\mathbf{U}}\right), \end{gathered} \tag{15} $$

where $\Delta\mathbf{U}^{(i)}$ is the correction of displacements in the ith Newton-Raphson iteration of the 1st substep:

$$ {}^{t+\Delta t/2}\mathbf{U}^{(i)} = {}^{t+\Delta t/2}\mathbf{U}^{(i-1)} + \Delta\mathbf{U}^{(i)}. \tag{16} $$

The velocities and accelerations at the time $t + \Delta t/2$ are computed according the formulas [2]:

$$ {}^{t+\Delta t/2}\dot{\mathbf{U}} = \left({}^{t+\Delta t/2}\mathbf{U} - {}^t\mathbf{U}\right)\frac{4}{\Delta t} - {}^t\dot{\mathbf{U}}, \tag{17} $$

$$ {}^{t+\Delta t/2}\ddot{\mathbf{U}} = \left({}^{t+\Delta t/2}\mathbf{U} - {}^t\mathbf{U} - \frac{\Delta t}{2}{}^t\dot{\mathbf{U}}\right)\frac{16}{\Delta t^2} - {}^t\ddot{\mathbf{U}}. \tag{18} $$

The three-point Euler backward method is employed in the 2nd substep with governing equations [3]:

$$\left(\frac{9}{\Delta t^2}\mathbf{M} + {}^{t+\Delta t}\mathbf{K}^{(i-1)}\right)\Delta\mathbf{U}^{(i)} = {}^{t+\Delta t}\mathbf{R} - {}^{t+\Delta t}\mathbf{F}^{(i-1)}$$
$$- \mathbf{M}\left(\frac{9}{\Delta t^2}{}^{t+\Delta t}\mathbf{U}^{(i-1)} - \frac{12}{\Delta t^2}{}^{t+\Delta t/2}\mathbf{U}^{(i-1)} + \frac{3}{\Delta t^2}{}^{t}\mathbf{U} - \frac{4}{\Delta t}{}^{t+\Delta t/2}\dot{\mathbf{U}} + \frac{1}{\Delta t}{}^{t}\dot{\mathbf{U}}\right), \tag{19}$$

where $\Delta\mathbf{U}^{(i)}$ is the correction of displacements in the ith Newton-Raphson iteration of the 2nd substep:

$$^{t}\mathbf{U}^{(i)} = {}^{t}\mathbf{U}^{(i-1)} + \Delta\mathbf{U}^{(i)}. \tag{20}$$

The velocities and accelerations at the time $t + \Delta t$ are updated using formulas [3]:

$$^{t+\Delta t}\dot{\mathbf{U}} = \frac{1}{\Delta t}{}^{t}\mathbf{U} - \frac{4}{\Delta t}{}^{t+\Delta t/2}\mathbf{U} + \frac{3}{\Delta t}{}^{t+\Delta t}\mathbf{U}, \tag{21}$$

$$^{t+\Delta t}\ddot{\mathbf{U}} = \frac{1}{\Delta t}{}^{t}\dot{\mathbf{U}} - \frac{4}{\Delta t}{}^{t+\Delta t/2}\dot{\mathbf{U}} + \frac{3}{\Delta t}{}^{t+\Delta t}\dot{\mathbf{U}}. \tag{22}$$

4 Numerical Examples

The linearly increasing force with increment $\Delta\mathbf{P}$ in time step Δt is applied for three structures with different geometry and boundary conditions. Central difference and Bathe integration schemes are employed for all examples to get a dynamic response on the applied loads. An isotropic material with parameters in Table 1 is used in calculations. The initial thickness of the shell element $h = 0.1$ m in all examples.

Conditional parameter uTH determines whether the thickness is updated during the calculations.

Table 1. Material parameters.

Young's modulus, N/m^2	$75 \cdot 10^9$
Poisson's ratio	0.32
Mass density, kg/m^3	2700

4.1 Tensioned Beam

A beam is loaded at the ends with linearly increasing force **P** (Fig. 2). The highlighted part of the beam in Fig. 2(a) is simulated using finite element method with the symmetry conditions applied for the thick lines in Fig. 2(b). The geometry of the beam: $a = 0.2$ m, $L = 1$ m.

As the in-plane load is applied, all elements become thinner in the deformed configuration during dynamic analysis (Fig. 3). The thickness of the elements near the end is reduced earlier than the thickness of the elements in the center due to the load type.

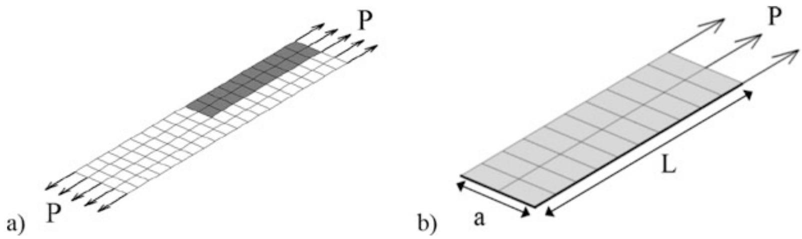

Fig. 2. (a) Initial geometry and loads. (b) Finite element mesh for 1/4 of the beam.

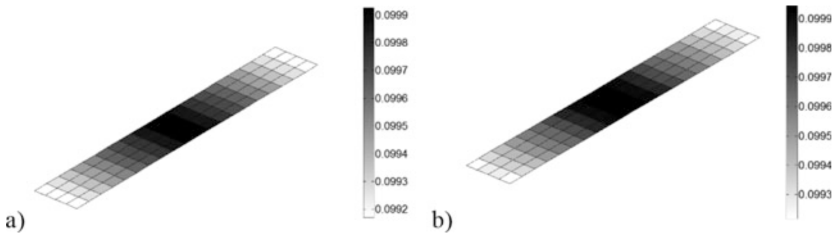

Fig. 3. Shell thickness at time $t = 2 \cdot 10^{-4}$ s: (a) central difference scheme ($\Delta t = 10^{-5}$ s, $\Delta P = 10^6$ N), (b) Bathe scheme ($\Delta t = 2 \cdot 10^{-5}$ s, $\Delta P = 2 \cdot 10^6$ N).

If the thickness update is applied, the x displacements at the end of the beam reach higher values compared with the displacements computed otherwise (Fig. 4). This is caused by the fact that the deformed beam becomes thinner and weaker than the beam with constant thickness.

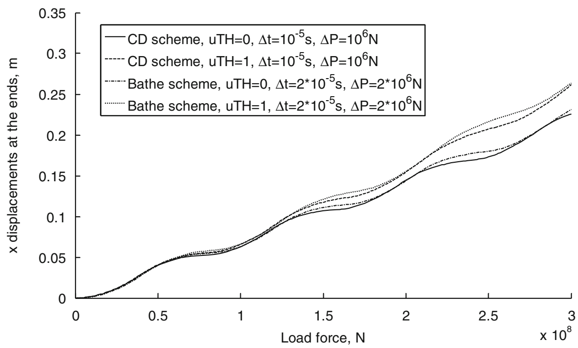

Fig. 4. x displacement at the end of the beam. Parameter $uTH = 0$ if shell thickness is not updated and $uTH = 1$ if shell thickness is updated, CD – central difference scheme.

4.2 Fixed Beam with Central Load

A beam is loaded in the center with linearly increasing force **P**. All degrees of freedom are constrained at both ends of the beam (dash lines in Fig. 5(a)). The highlighted part of the beam in Fig. 5(a) is simulated using finite element method with the symmetry conditions applied for the thick lines in Fig. 5(b). The geometry of the beam: $a = 0.2\,\mathrm{m}$, $L = 1\,\mathrm{m}$.

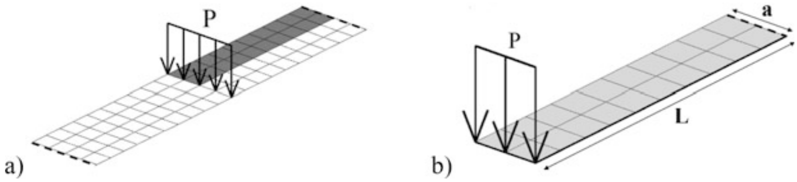

Fig. 5. (a) Initial geometry and loads. (b) Finite element mesh for 1/4 of the beam.

The shell thickness is reduced for the elements near the loaded and constrained nodes (Fig. 6). Under this type of load the behavior of the structure is mainly governed by the rotational displacements without significantly affecting the area of element. The vertical displacements computed with the updated thickness have minor differences compared with the displacements computed otherwise (Fig. 7).

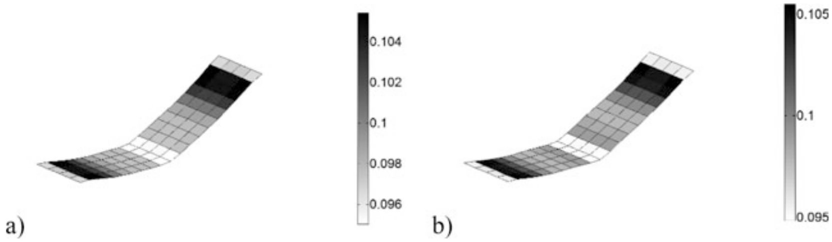

Fig. 6. Shell thickness at time $t = 10^{-3}\,\mathrm{s}$: (a) central difference scheme ($\Delta t = 10^{-5}\,\mathrm{s}$, $\Delta P = 5 \cdot 10^{5}\,\mathrm{N}$), (b) Bathe scheme ($\Delta t = 2 \cdot 10^{-5}\,\mathrm{s}$, $\Delta P = 10^{6}\,\mathrm{N}$).

If long-time durations are considered with increasing forces, the central difference scheme becomes unstable (Fig. 7). The reduced time step should be employed to maintain stability of the scheme. However, the reduction of time step increases computational cost and is not desirable.

4.3 Pinched Cylinder with End Diaphragms

A cylindrical shell is pinched by two opposite forces applied at the middle section. The cylinder is closed at both ends by rigid diaphragms which constrain translations in **X**

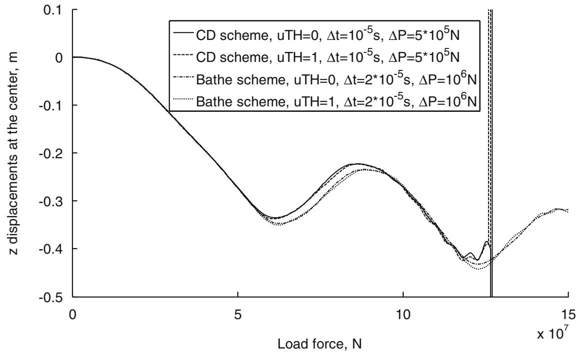

Fig. 7. z displacement at the center of the beam. Parameter $uTH = 0$ if shell thickness is not updated and $uTH = 1$ if shell thickness is updated, CD – central difference scheme.

and **Y** directions and rotations about the **X** axis at the edges. This test involves inextensional bending and complex membrane states of stress [13]. For example, the elements near the pinched node undergo warping effects. As the symmetric load is applied, only the highlighted part of the cylinder (Fig. 8(a)) is simulated using finite element method with linearly increasing force **P** and appropriate symmetry conditions applied for the thick lines in Fig. 8(b). The geometry of the cylinder: $r = 1$ m, $L = 1$ m.

The shell thickness is thinner than the initial thickness for the elements near the pinched node and thickens farther from the pinched zone (Fig. 9). The thickness at the sides of the cylinder are not affected significantly. The shell thickness computed using Bathe implicit integration scheme varies in a wider range compared to the thickness computed using central difference scheme under the same load and boundary conditions.

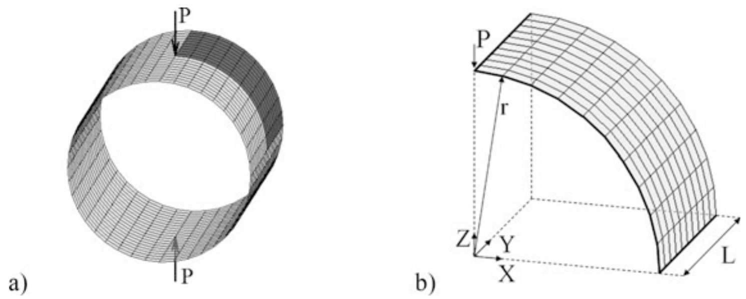

Fig. 8. (a) Initial geometry and loads. (b) Finite element mesh for 1/8 of the cylinder.

If the thickness update is applied, the deflections at the pinched node are smaller compared with the deflections computed otherwise (Fig. 10). However, these differences are not significant as there are no evident boundaries between the displacement curves computed with constant and updated thickness assumptions in the analyzed period under the considered boundary and load conditions.

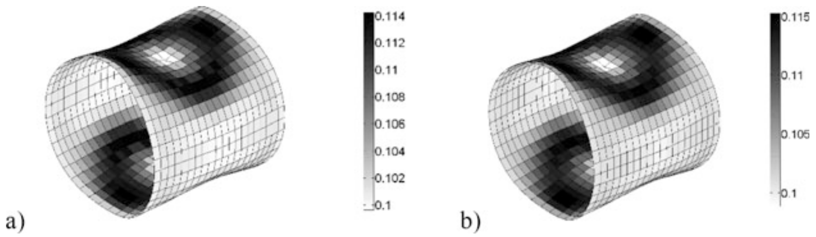

Fig. 9. Shell thickness at time $t = 2 \cdot 10^{-3}$ s: (a) central difference scheme ($\Delta t = 10^{-5}$ s, $\Delta P = 2 \cdot 10^5$ N), (b) Bathe scheme ($\Delta t = 2 \cdot 10^{-5}$ s, $\Delta P = 4 \cdot 10^5$ N).

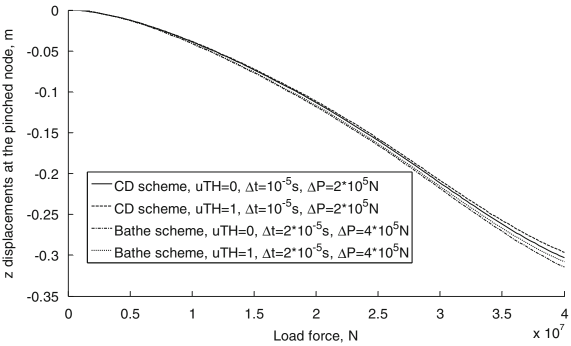

Fig. 10. z displacement at the pinched node. Parameter $uTH = 0$ if shell thickness is not updated and $uTH = 1$ if shell thickness is updated, CD – central difference scheme.

5 Conclusions

The objective of this paper was to focus on the shell thickness update in the dynamic analysis with the updated Lagrangian formulation. Explicit central difference and implicit Bathe time integration schemes were implemented to compare the response of the structure. Although the time step used in numerical examples for the Bathe implicit analysis was twice the time step used in explicit analysis, the implicit Bathe time integration scheme has considerably higher computational cost. This is caused by the fact that the stiffness matrix and internal force vector of the structure are reassembled at each iteration. However, this scheme is stable when the central difference scheme fails as in the example for the vertically loaded beam with the fixed ends.

If the thickness of the element is updated, the changes in geometry of the structure are taken into consideration. For the examples with out-of-plane loads, the behavior is governed by rotational displacements and the changes in element area and therefore thickness are minor. If element undergoes large deformations, the stiffness of the element is updated by reducing its thickness and the displacements reach higher values.

References

1. Bathe, K.J.: Finite Element Procedures. Prentice Hall, Englewood Cliffs (1996)
2. Bathe, K.J., Baig, M.M.I.: On a composite implicit time integration procedure for nonlinear dynamics. Comput. Struct. **83**, 2513–2524 (2005)
3. Bathe, K.J.: Conserving energy and momentum in nonlinear dynamics: a simple implicit time integration scheme. Comput. Struct. **85**, 437–445 (2007)
4. Echter, R., Oesterle, B., Bischoff, M.: A hierarchic family of isogeometric shell finite elements. Comput. Methods Appl. Mech. Eng. **254**, 170–180 (2013)
5. Miller, K., Joldes, G., Lance, D., Wittek, A.: Total Lagrangian explicit dynamics finite element algorithm for computing soft tissue deformation. Commun. Numer. Meth. Eng. **23**, 121–134 (2007)
6. Nguyen-Van, H., Mai-Duy, N., Tran-Cong, T.: An improved quadrilateral flat element with drilling degrees of freedom for shell structural analysis. CMES-Comp. Model. Eng. **49**(2), 81–110 (2009)
7. Oñate, E., Cendoya, P., Miquel, J.: Non-linear explicit dynamic analysis of shells using the BST rotation free triangle. Eng. Comput. **19**, 662–706 (2002)
8. Oñate, E.: Structural Analysis with the Finite Element Method. Linear Statics. Volume 2. Beams, Plates and Shells. Lecture Notes on Numerical Methods in Engineering and Sciences. Springer, Berlin (2013)
9. Sussman, T., Bathe, K.J.: 3D-shell elements for structures in large strains. Comput. Struct. **122**, 2–12 (2013)
10. Tabiei, A., Tanov, R.: Sandwich shell finite element for dynamic explicit analysis. Int. J. Numer. Meth. Eng. **54**, 763–787 (2002)
11. Voyiadjis, G.Z., Woelke, P.: Elasto-Plastic and Damage Analysis of Plates and Shells. Springer, Berlin (2008)
12. Zienkiewicz, O.C., Taylor, R.L.: The Finite Element Method for Solid and Structural Mechanics. Elsevier, Amsterdam (2005)
13. Wisniewski, K.: Finite Rotation Shells. Basic Equations and Finite Elements for Reissner Kinematics. Lecture Notes on Numerical Methods in Engineering and Sciences. Springer, Berlin (2010)